Neutron study of the frustrated spinel compound $Mg_{1+t}Fe_{2-2t}Ti_tO_4$ ($t=0.55$)

I. Mirebeau,* G. Iancu, and M. Hennion
Laboratoire Léon Brillouin (Commissariat à l'Energie Atomique-Centre National de la Recherche Scientifique), CE-Saclay, F-91191 Gif-sur-Yvette, France

G. Gavoille and J. Hubsch
Laboratoire de Cristallographie et Modélisation des Matériaux Minéraux et Biologiques-Associé au CNRS-Université Henri Poincaré, Boite Postale 239, F-54506 Vandoeuvre les Nancy, France

(Received 18 June 1996)

We have performed neutron-diffraction and inelastic neutron-scattering measurements in the frustrated ferrimagnetic spinels $Mg_{1+t}Fe_{2-2t}Ti_tO_4$. The concentration studied here ($t=0.55$), is close to the percolation threshold for the dominant interaction. We observe spin fluctuations of short-range correlated spins, which persist well above the Néel temperature T_N. Below T_N, these dynamical correlations coexist and compete with static domains, ordered on a longer scale. In this inhomogeneous system, we measure several energy levels for the spin excitations, corresponding to different length scales for the spin correlations. The neutron results are discussed in comparison with magnetic measurements, performed on the same sample. [S0163-1829(96)01646-3]

I. INTRODUCTION

The spinel compounds of cubic structure $(A_xD_{1-x})(B_yD_{1-y})_2O_4$, where A and B correspond to magnetic atoms, and D are diamagnetic ones, show an interesting problem of frustration together with site dilution. The spinel lattice has been intensively studied by theoreticians, considering first-neighbor antiferromagnetic (AF) interactions J_{AA}, J_{BB}, and J_{AB}. The A and B sublattices exhibit different topological features.[1] In the A sublattice, of tetrahedral symmetry, AF interactions do not yield any frustration, and magnetic dilution is a simple percolation problem. By contrast, in the B sublattice of octahedral symmetry, AF interactions yield a topological frustration, like in the Kagomé and pyrochlore lattices.[2] The B dilution partly raises the degeneracy, leading to a spin-glass state. When both sublattices are full, the dominant AF interaction J_{AB} impose a casual ferrimagnetic behavior. For intermediate dilutions, one may observe either a semispin glass, or a classical spin glass. Therefore, the phase diagram at 0 K may present a great variety of magnetic phases, whose extension is controlled by the concentrations of the magnetic atoms and by the strength of the exchange interactions.[1,3]

From an experimental point of view, several questions can be raised. What is the nature of the low-temperature states and of the magnetic transitions? Are there fundamental differences with the metallic frustrated systems? The $(Fe_xMg_{1-x})(Fe_{2y}Mg_{2-2y-t}Ti_t)O_4$ system was already studied by magnetic and Mössbauer measurements.[4,5] For $t=0$, the compound $FeMg_2O_4$ is a partly inverted spinel ($x=1/3$, $y=2/3$), which behaves as a collinear ferrimagnet with a Néel temperature of 680 K. When the B sites are diluted by Ti, according to Monte Carlo simulations of Scholl and Binder,[6] the dilution curve intersects the percolation limit for J_{AB} at the value $t_1=0.68$. If first neighbor AA and BB interactions are also considered,[7] this intersection is found at a higher value $t_{II}=0.83$, which corresponds to the upper limit for any cooperative type of ordering.

We present here a neutron study of a $t=0.55$ sample situated just beyond t_I, namely a so-called ''semispin glass.'' In this sample, Mössbauer and magnetization measurements,[4] suggested the existence of two ''transitions'' with decreasing the temperature: a first transition at T_N ($T_N=164$ K), from a paramagnet to a collinear ferrimagnet, then at a lower temperature T_F ($T_F=25$ K), a second transition to a mixed state where long-range order and local canting seemed to coexist. Anomalies of the spin-wave stiffness constant were also observed.[8] The neutron probe yields new informations, since it allows us to investigate the magnetic correlations on the scale of 2–200 Å, in a range between the local (Mössbauer) and the macroscopic (magnetization) probes. Moreover, the local spin fluctuations may be studied by inelastic neutron scattering.

We have divided this paper in six sections. In Sec. II, we present the results about the mean chemical and magnetic order, obtained by neutron diffraction. In Sec. III, we analyze the neutron diffuse scattering. This yields the temperature and field evolution of the short-range magnetic correlations. We have studied the dynamical character of these correlations by time-of-flight neutron scattering (Sec. IV). In Sec. V, we propose a phenomenological description of the system, trying to account for all experimental results. In the Conclusion (VI), we compare our results with some in other metallic and insulating systems, and discuss them in the frame of the available theoretical models. The study of four other samples, in the concentration range $0.5<t<0.7$ encompassing t_I, will be detailed elsewhere, but some results will be briefly mentioned throughout this paper.

II. NEUTRON DIFFRACTION

We have measured the neutron-diffraction spectra on the spectrometer 3T2 of the reactor Orphée, with a neutron wavelength of 1.227 Å. The spectra were registered at two

temperatures. One at 300 K, namely above T_N, yields the nuclear structure, the other one at 8 K (below T_F) provides in addition the mean magnetic moments in the mixed phase.

The spectra were analyzed using the Rietveld method, in the space group $Fd3m$, assuming that Ti occupies the B sublattice only. At 300 K, we refined the lattice parameter a, the z coordinates of the atomic positions, the Debye Waller factors, and the Fe/Mg occupancy. The nuclear profile factors R are around 2. For the compound $t=0.55$, a is equal to 8.4266(1) Å at 300 K and to 8.4173(1) Å at 8 K. The occupancies probabilities of Fe on the A and B sublattices are, respectively, $x=0.328(8)$, $y=0.286(4)$ (with $x+2y=2-2t$). These values are close but still different from the values predicted for a random dilution ($x=0.368$, $y=0.266$), which shows that Fe slightly prefers the B sites. This could be related to some local ordering in this sublattice as shown in Sec. III. The study of the other samples ($t=0.5,0.6,0.65,0.7$) confirms these observations, and shows that a varies linearly with t.

Magnetic Rietveld refinements were performed assuming a mean collinear structure, and considering the magnetic diffuse scattering as a background. The magnetic R value is equal to 9.4 for the $t=0.55$ sample. At 8 K we obtain the absolute moment values $M_A=2.27+-0.34\mu_B$/Fe and $M_B=3.34+-0.31\mu_B$/Fe, with the assumption that all the iron spins contribute to the ferrimagnetic order. The Ti dilution yields a decrease of the ordered Fe spins with respect to the value in the $FeMg_2O_4$ compound ($M=5\mu_B$ as expected for Fe^{3+} ions).[9] The values found for the magnetic moments clearly show that the assumption of a collinear ground state does not hold. This is confirmed by the study of the other compounds. No ordered moment is found for the sample $t=0.7$, situated above t_1.

A strong diffuse scattering, whose intensity increases with increasing t, is observed in the neighborhood of the ferrimagnetic Bragg peaks. It is analyzed in detail in the following section.

III. NEUTRON DIFFUSE SCATTERING

We studied the magnetic scattering near the (111) Bragg peak on the powder diffractometer G6-1 at Orphee, equipped with a linear multidetector of 400 cells. The large neutron wavelength (4.744 Å), permitted us to focus on this peak with a good resolution. Spectra recorded between 460 and 8 K were corrected from background, sample absorption, and cell efficiency. We performed the measurements in zero field and in applied field, in the range 0–12 kOe.

A. Temperature dependence of the magnetic correlations

The intensity of the (111) diffraction peak strongly increases below T_N ($T_N=164$ K). A diffuse signal, centered at the (111) peak position, is clearly visible and persists well above T_N, up to about 440 K, as shown in Fig. 1. Above 440 K, the diffuse signal becomes temperature independent, suggesting its purely nuclear origin. In this temperature range, we observe diffuse maxima on each side of the (111) Bragg peak, due to chemical short-range order (SRO) on a very local scale. Since the A sublattice is only occupied by Mg and Fe atoms, whose neutron chemical contrast is very small, we attribute these maxima to some heterocoordination in the

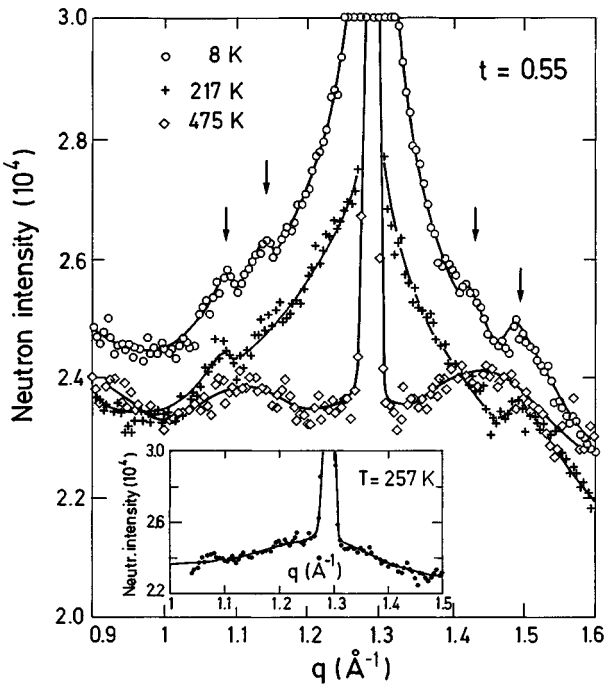

FIG. 1. Intensity of the (111) Bragg peak for several temperatures. The solid line is a guide for the eye. In the inset, a typical fit of the data, using Eq. (2a).

B sublattice. Fe and Mg are likely mostly surrounded by Ti atoms as nearest neighbors. For $t=0.5$, an ordered compound where the Ti atoms occupy one of the four B sites, could exist with a space group $P4_132$.[10] This would yield (110) and (200) substructure peaks, with positions close to the observed maxima. In a disordered compound, we also expect that Ti^{4+} ions would be more surrounded by Fe or Mg than by Ti, in order to keep some local electric neutrality.

Below 300 K, in the limited q range of the analysis, ($1<q<1.5$ Å^{-1}), this local nuclear contribution may be approximated by a linear q dependence. Therefore, we analyzed the total intensity as the sum of three terms. A diffraction peak $I_1(q)$ takes into account the long-range nuclear and magnetic order. A diffuse peak $I_2(q)$ describes the short-range magnetic correlations, and a sample ''background'' term $I_3(q)$ involves incoherent scattering and the very local ordering. At low temperature, small maxima at the limit of the statistical accuracy, seem to be superimposed on the diffuse peak. This suggests a short-range helical ordering like in manganese chromite[11] and cobalt ferrites.[12] This was not taken into account in the analysis. $I_1(q)$ is expressed as a Gaussian of intensity I_G and width w, centered at the Bragg peak position τ,

$$I_1(q)=I_G\exp\left[\frac{-(q-\tau)^2}{w^2}\right]. \tag{1a}$$

For the (111) peak, the magnetic contribution to the quantity I_G is proportional to the square of the structure factor F_{111}:

$$\langle F_{111}\rangle^2=\tfrac{2}{3}|8yM_B+4x\sqrt{2}M_A|^2f^2(q), \tag{1b}$$

where $f(q)$ is the Fe^{3+} form factor. For the diffuse term, we consider two possible functions to describe the short-range

correlations, either $f(r)=\exp(-\kappa r)$ or $f(r)=\exp(-\kappa r)/r$, where $\xi=\kappa^{-1}$ is the correlation length. The Fourier transform of $f(r)$ yields a squared Lorentzian term in the first case, and a simple Lorentzian in the second one, both being centered at the reciprocal points $\boldsymbol{\tau}$. For a polycrystal, these Fourier transforms must be averaged over all directions of $\boldsymbol{\tau}$ with respect to the scattering vector $\mathbf{q}$.[13] This yields

$$I_2(q)=\frac{I_L}{q\cdot\tau}\left[\frac{1}{(q-\tau)^2+\kappa^2}-\frac{1}{(q+\tau)^2+\kappa^2}\right]$$

$$\text{for } f(r)=\exp(-\kappa r), \qquad (2a)$$

$$I_2(q)=\frac{I_L\cdot\kappa}{q}\ln\left[\frac{(q+\tau)^2+\kappa^2}{(q-\tau)^2+\kappa^2}\right] \quad \text{for } f(r)=\exp(-\kappa r)/r, \qquad (2b)$$

where q and τ are the moduli of the vectors. Expressions (2a) and (2b) are convoluted to the experimental resolution $I_1(q)$, where the width of the resolution peak ($w_0=9.7\times10^{-3}$ Å^{-1} at the 111 peak position) is checked by measuring a standard zeolithe sample. The sample background $I_3(q)$ is expressed as

$$I_3(q)=a_1+a_2(q-q_{\min}), \qquad (3)$$

where $q_{\min}=1.04$ Å^{-1}. The total intensity $I(q)=I_1(q)+I_2(q)f^2(q)+I_3(q)$, is fitted to the data with I_G, I_L, w, κ, a_1, and a_2 as parameters (inset Fig. 1). The Fe^{3+} form factor $f(q)$ is approximated to $\exp(-0.051q^2)$ in our experimental q range.[14] Both types of $f(r)$ functions fit the data very well, and yield very similar dependences for the fitted parameters I_G, I_L, and w. The main difference comes from the value of the correlation length, which is much higher when fitting with Eq. (2b) than with Eq. (2a).

The temperature dependence of the fitted parameters is shown in Figs. 2 and 3. With decreasing T, the Gaussian intensity I_G increases slowly and linearly, as expected from Debye-Waller effects. At T_N, due to an additional magnetic contribution, it changes its slope and starts to increase more steeply, keeping a linear-T dependence. I_G shows a maximum at T_F then decreases. The Gaussian width w is equal to the resolution limit w_0 in the high- and low-temperature ranges, and shows a slight maximum at T_N, due to critical fluctuations. Keeping w equal to w_0 in the fit does not change the results significantly. The parameters I_L and ξ related to the diffuse term start to increase well above T_N, show a plateau or a rounded maximum at T_N, and finally increase below T_F. The ξ value changes by almost one order of magnitude, depending on the chosen function but its T dependence is the same for both functions. Clearly when the temperature decreases, there is a competition between the growing of the short-range correlations, and the static component related to the mean magnetic order.

The local a_1 term varies with temperature like the Bragg term I_G when fitting with Eq. (2a), whereas it varies like I_L when fitting with Eq. (2b), the slope a_2 remaining almost T independent. This shows that the local term also contains a magnetic contribution, which could have two origins (i) the presence of isolated or almost uncorrelated fluctuating spins, (ii) in the static ordered medium, a chemical contrast between Fe and the nonmagnetic atoms. This latter contribution, similar to the chemical one, is expected in any disordered magnetic alloy, even for a pure collinear order.[15] It should roughly increase with decreasing T as the squared magnetization of one sublattice.

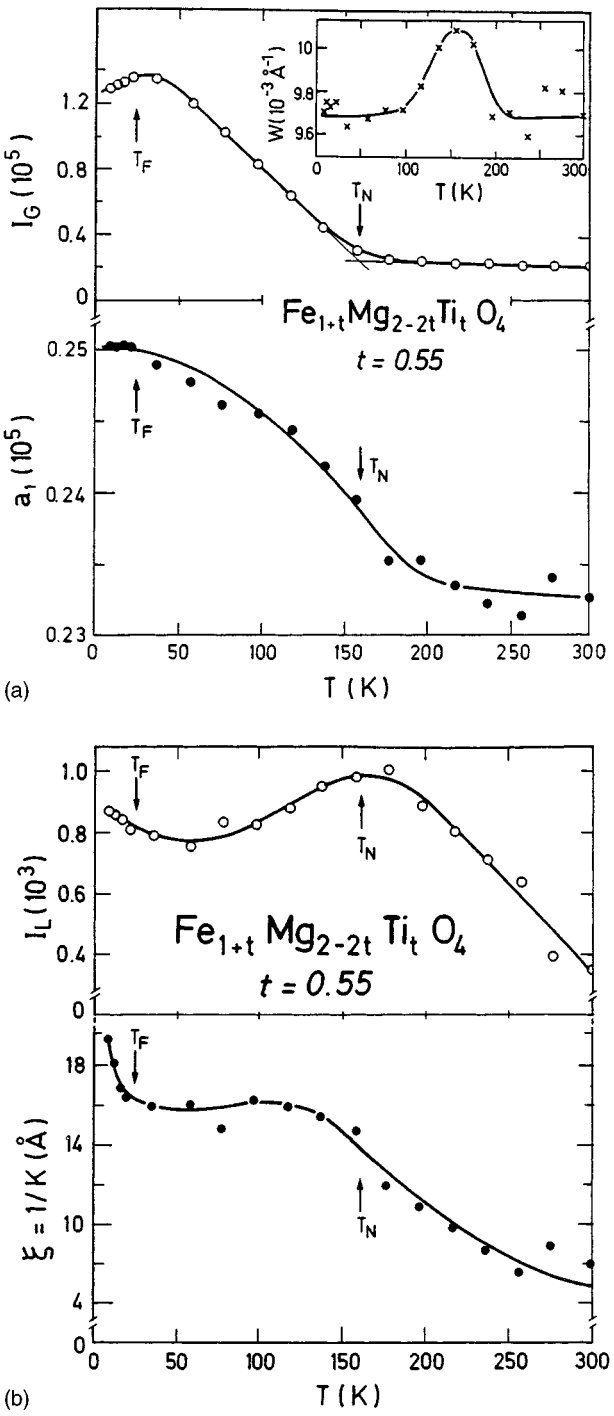

FIG. 2. Temperature dependence of the parameters which describe the magnetic correlations, assuming $\langle S_0S_1\rangle=\exp(-\kappa r)$ [Eq. (2a)]. (a) the Gaussian intensity I_G, the Gaussian width w_0 (in inset), and the local ''background'' term a_1 (b), the diffuse intensity I_L and the correlation length ξ ($\xi=1/\kappa$).

At the (220) peak position, the magnetic Bragg intensity is proportional to $(2xM_A)^2$. By combining data on (220) and (111) peaks [Eq. (1b)], we obtained the temperature dependences of the sublattices magnetizations xM_A and yM_B (Fig.

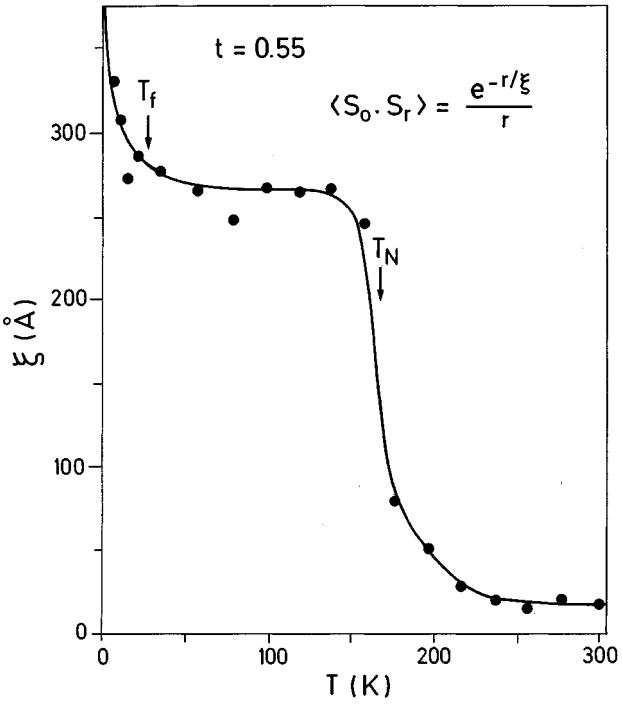

FIG. 3. Temperature dependence of the correlation length ξ, assuming $\exp(-\kappa r)/r$ correlation decay [Eq. 2(b)].

4). At 8 K, the ratio M_A/M_B (1.48), is in agreement with the value given by the Rietveld refinement. From these results we can evaluate the magnetization M_0, proportional to $2yM_B - xM_A$. The M_0 value deduced from the neutron data at 8 K (36 ± 7 emu/g) is higher than the value obtained from high-field magnetization (20 emu/g). However, both evaluations scale very well in the whole temperature range, as shown in the inset of Fig. 4.

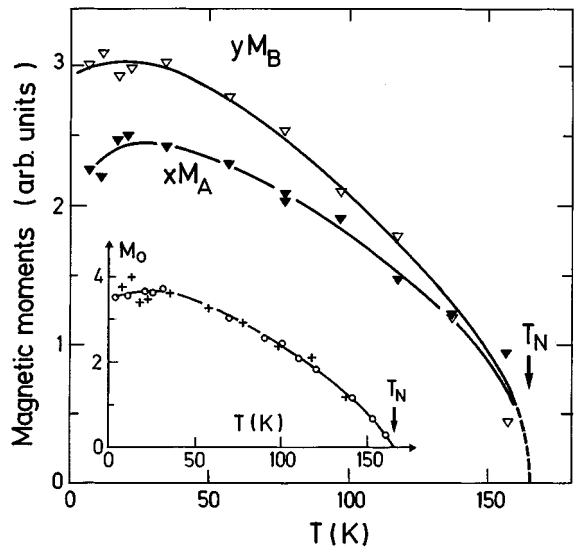

FIG. 4. Temperature dependence of the magnetic moments on the A and B sublattices. The magnetization M_0, deduced from neutron (+) and magnetic (○) data, is shown in inset. The two determinations of M_0 are scaled to each other at 100 K. Solid lines are guides for the eye.

B. Field dependence of the magnetic correlations

To study the spin reorientations in applied field, we used two experimental setups. (1) with a horizontal field parallel to the scattering vector $\mathbf{q}_\tau$ of the (111) Bragg peak ($|\mathbf{q}_\tau| = \tau$), we selected the transverse correlations $2T$, due to spin components perpendicular to the applied field. (2) with a vertical field (perpendicular to the scattering plane), we measured the sum $L+T$, where L and T correspond to correlations along and perpendicular to the field, respectively. We analyzed the data like in zero field, using a double Lorentzian description for the diffuse scattering [Eq. (2a)].

The competition between SRO and LRO, observed in zero field with decreasing temperature, remains clearly visible in applied field. As in zero field, three main temperature regions can be defined: (1) $T > T_N$ where the effects of the applied field are negligible. (2) $T_F < T < T_N$, where a progressive spin alignment occurs, with a transverse correlation length ξ varying with $1/\sqrt{H}$ [Fig. 5(c)]. (3) $T < T_F$, where the field effects are very strong and comparable to those observed in usual ferromagnets. The field dependence of the Bragg intensity below T_N shows the existence of a technical saturation field $H_{\text{sat}} = 500$ Oe for which most of the spin alignment occurs, in good agreement with magnetic measurements [inset of Fig. 5(a)].

In a horizontal field $\mathbf{H} \| \mathbf{q}_\tau$ [Fig. 5(a)], the Bragg intensity I_G strongly decreases with increasing H for $H < H_{\text{sat}}$. Above H_{sat}, I_G decreases much more slowly and tends to the ''nuclear'' value I_{nuc} measured for $T > T_N$. The diffuse intensity I_L is almost field independent for $H < H_{\text{sat}}$ then starts to decrease slowly with increasing H [Fig. 5(b)]. In a vertical field $\mathbf{H} \perp \mathbf{q}_\tau$ (Fig. 6), I_G strongly increases for $H < H_{\text{sat}}$, then shows a knee and increases much more slowly at low temperature. The variation of the Bragg intensity for $H < H_{\text{sat}}$ at low temperature roughly corresponds to that expected for the alignment of random ferromagnetic domains ($I = I_{\text{nuc}} + 2/3 I_{\text{mag}}$ for $H = 0$, $I = I_{\text{nuc}} + I_{\text{mag}}$ for $H \geqslant H_{\text{sat}}$ perpendicular to $\mathbf{q}_\tau$, $I = I_{\text{nuc}}$ for $H \geqslant H_{\text{sat}}$ along $\mathbf{q}_\tau$), where I_{nuc} and I_{mag} are, respectively, the nuclear and the magnetic contributions to the Bragg intensity. In contrast, the spins or spin components which give rise to the diffuse scattering align much more slowly with H, as expected for short-range correlations or fluctuating spins.

IV. TIME-OF-FLIGHT NEUTRON SCATTERING

In the above experiments we did not analyze the energy of the scattered neutrons. Energy-integrated measurements yield the instantaneous correlations. Since the diffuse magnetic scattering appears well above T_N and is hardly affected by the applied field, it could be related to fluctuations of the short-range correlated spins. We have therefore performed time-of-flight measurements to analyze these fluctuations in more detail. Measurements were performed on the time-of-flight (TOF) spectrometer MIBEMOL of the reactor ORPHEE, with an incident wavelength of 5.5 Å, and an energy resolution of 0.01 THz (full width at half maximum). Spectra registered between 10 and 300 K were corrected from the (elastic) background of the cryostat. The detectors efficiency and the resolution function were determined with a vanadium sample. A typical TOF spectrum displays three main regions, according to the energy range considered. The

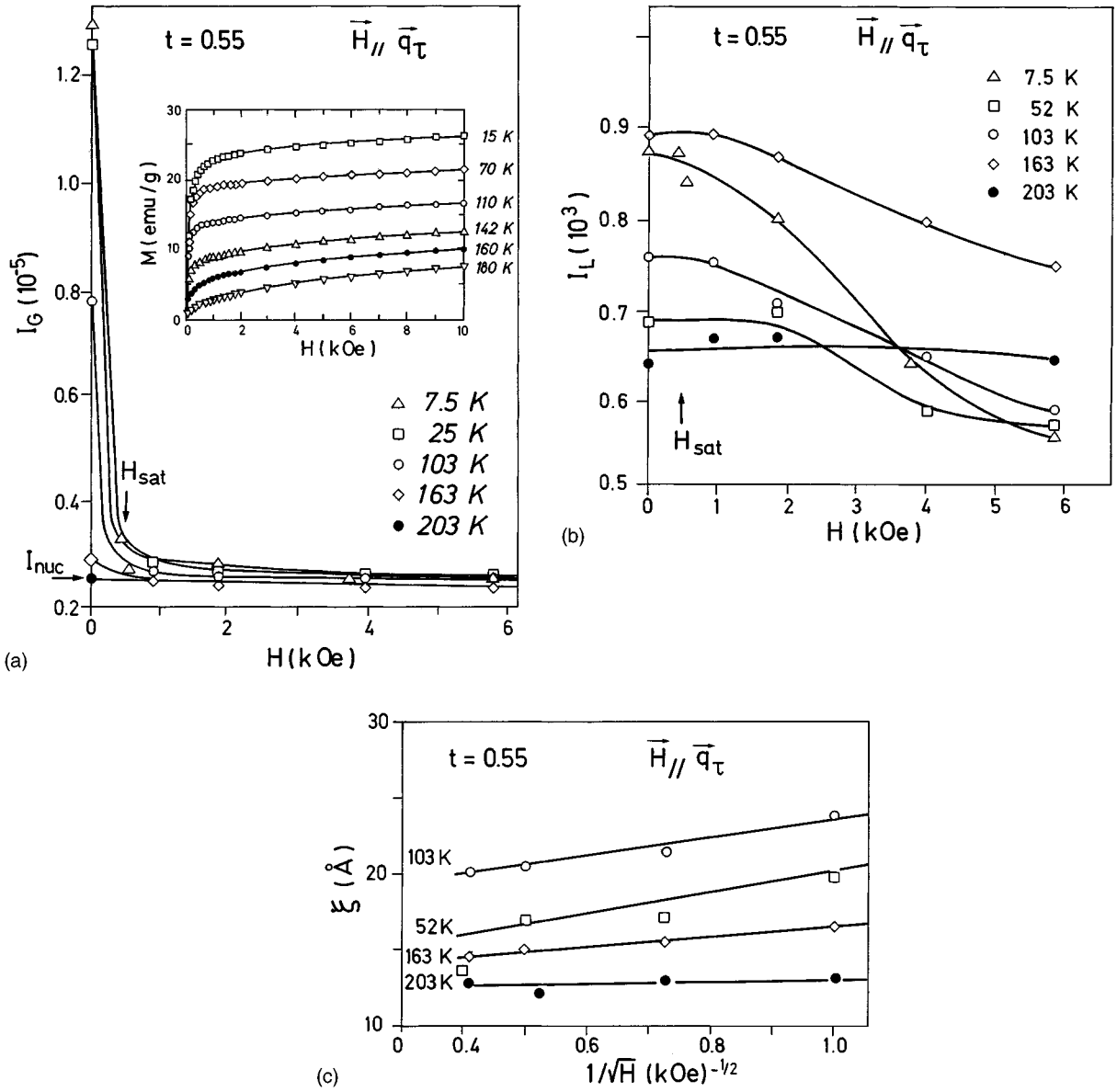

FIG. 5. Dependence of the fitted parameters with the magnetic field **H**, applied parallel to $\mathbf{q}_\tau$ (a) the Gaussian intensity I_G versus H. (b) the diffuse intensity I_L versus H. (c) the correlation length ξ versus $1/\sqrt{H}$. The fit is performed with Eq. (2a). The field dependence of the mean magnetization is shown in the inset of (a) for several temperatures.

''elastic'' region corresponds to scattering processes of energy limited by the spectrometer resolution. The ''inelastic'' region at high energies is mostly due to phonons. The ''quasielastic'' region, in the small energy range near the elastic peak, is attributed to spin fluctuations.

A TOF spectrum at 50 K is shown in Fig. 7, focusing on the quasielastic region. In this energy range, we analyzed the spectra as the sum of five contributions, namely the elastic peak (of intensity $c_{\rm el}$), *two* quasielastic signals of widths Γ_1 and Γ_2 ($\Gamma_1 \gg \Gamma_2$), a phonon term (fitted with a αt^{-4} law) and a small time-independent background. For each quasielastic signal, we describe the spectral function of the spin fluctuations by a Lorentzian, multiplied by a Bose factor. Taking $\hbar=1$, the corresponding cross section:

$$S(q,\omega)=\frac{1}{\pi}\frac{\Gamma}{\Gamma^2+\omega^2}\frac{\omega}{e^{\omega/kT}-1}\chi(q) \qquad (4)$$

is convoluted to the resolution function. In Eq. (4), ω is the energy transfer ($\omega>0$ corresponding to a neutron energy gain), and $\chi(q)$ is the static susceptibility. In the limit of small energy transfers ($\omega \ll kT$), the quantity $kT\chi(q)$ corresponds to the integration of the signal over all energies. It is therefore comparable to the intensity measured in diffraction. Considering the large number of fitted parameters (eight for each TOF spectrum), we could not determine χ_1 and χ_2 independently. Therefore we fixed the background and imposed a reasonable α value for the phonon contribution. Namely we fitted α at high temperature when it is very large and assumed a linear decrease with T. We also fitted the elastic region separately at the Bragg peak positions. We checked the reliability of this analysis by summing the data over well chosen TOF channels ($\Sigma_1,\Sigma_2,\Sigma_{\rm el}$ as shown in Fig. 7), where the two quasielastic signals and the elastic one are,

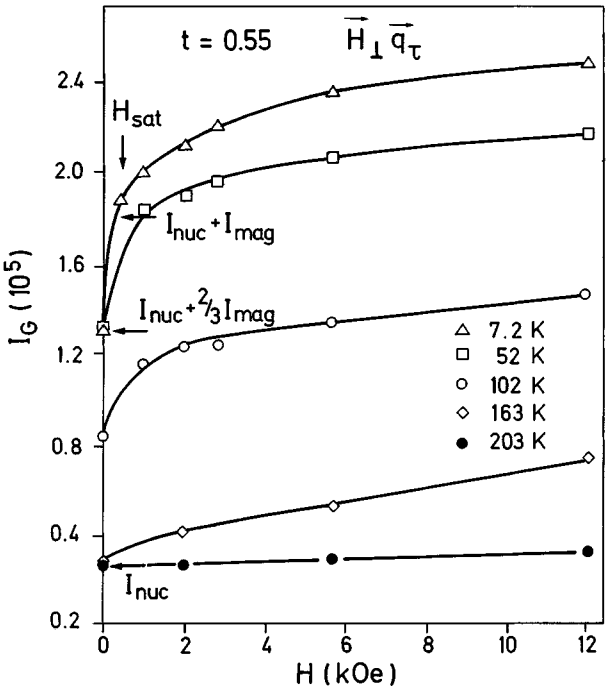

FIG. 6. Dependence of the Gaussian intensity I_G with the field **H**, applied perpendicular to $\mathbf{q}_\tau$.

respectively, dominant. These sums have the same q and T dependence as the corresponding intensities $kT\chi_1$, $kT\chi_2$, and $c_{\rm el}$.

In Figs. 8 and 9, the fitted parameters are plotted versus the (elastic) scattering vector q at 50 K. $c_{\rm el}(q)$ shows well defined maxima at the Bragg peaks, of nuclear and magnetic origins. At the same q values, the susceptibility χ_2 of the narrow quasielastic signal shows Lorentzian-like maxima. Its q dependence reflects the diffuse scattering measured in Sec. II. Therefore, this term is attributed to short-range ferrimagnetic correlations, with a correlation length ξ greater than the typical dimension of the unit cell. The quasielastic width Γ_2

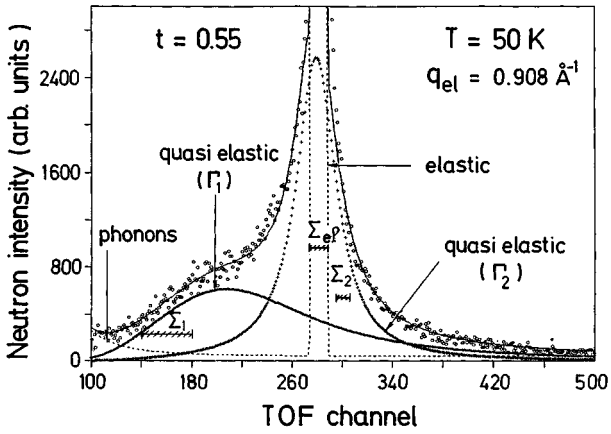

FIG. 7. Typical time-of-flight spectrum at $T=50$ K, focusing on the quasielastic region. The solid line is a fit to the data. The separate contributions to the cross section are also shown. The TOF intervals Σ_1, Σ_2, and $\Sigma_{\rm el}$ are the regions where the two quasielastic signals and the elastic one are, respectively, dominant, as described in the text.

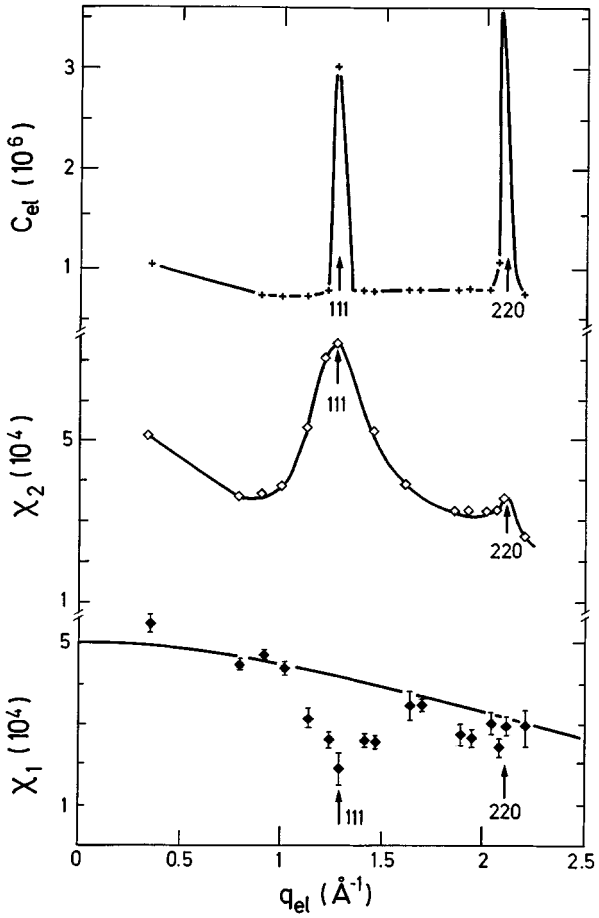

FIG. 8. Dependence of the parameters deduced from a fit of the TOF spectra at 50 K with the scattering vector $q_{\rm el}$. $c_{\rm el}$ is the elastic intensity, χ_1 and χ_2 are the static susceptibilities of the two quasielastic signals. The solid line for χ_1 is the square of the magnetic form factor of Fe^{3+} ions. The other solid lines are guides for the eye.

shows some minima at the q values where χ_2 is maximum, as expected for a correlated paramagnet.[16] For the same reason, it should tend to zero at very small q values. This could not be checked in our experiment.

The interpretation of the other quasielastic signal is more intricate due to the large value of the typical energy width Γ_1, which is around 5 to 15 meV, namely one order of magnitude greater than Γ_2. This leads to some difficulties in the analysis, since the q value varies significantly within a given TOF spectrum, measured at constant scattering angle. Moreover, the condition $\omega \ll kT$ is not satisfied at low temperature, so that the parameter $kT\chi_1$ cannot be simply related to an energy-integrated intensity and to spontaneous correlations. Therefore we will simply discuss the results in a qualitative way. By contrast with χ_2, the χ_1 parameter decreases with q, showing some small modulations with respect to the squared magnetic form factor $f^2(q)$. This suggests to attribute the large energy signal to spin-glass-like correlations or to very small spin clusters, with a correlation length comparable to the lattice parameter, so that the lattice periodicity would not be preserved. The structure factor of such clusters could present some modulations with respect to the form factor of

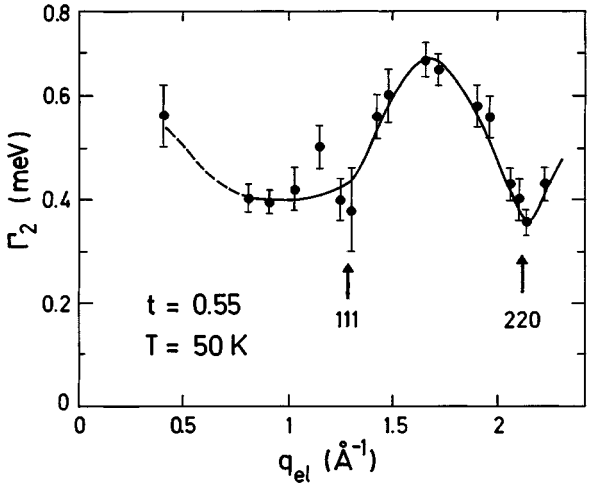

FIG. 9. Dependence of the quasielastic width Γ_2 with the scattering vector q_{el} at 50 K.

a single spin. A better analysis would require energy scans measured at constant q on a single crystal.

The parameters are plotted versus temperature in Figs. 10 and 11 for a q value of 0.908 $Å^{-1}$, aside the (111) peak. Similar variations are observed for other q values. With decreasing temperature, c_{el} strongly increases, much more than expected from Debye-Waller effects. In contrast the quantity $kT\chi_1$ related to almost uncorrelated spins continuously decreases. The quasielastic intensity $kT\chi_2$ starts to increase, due to the growing of the short-range correlations, then shows a round maximum and decreases too. The overall behavior of the parameters reflects a transfer from the quasielastic intensities to the ''elastic'' or resolution limited one,

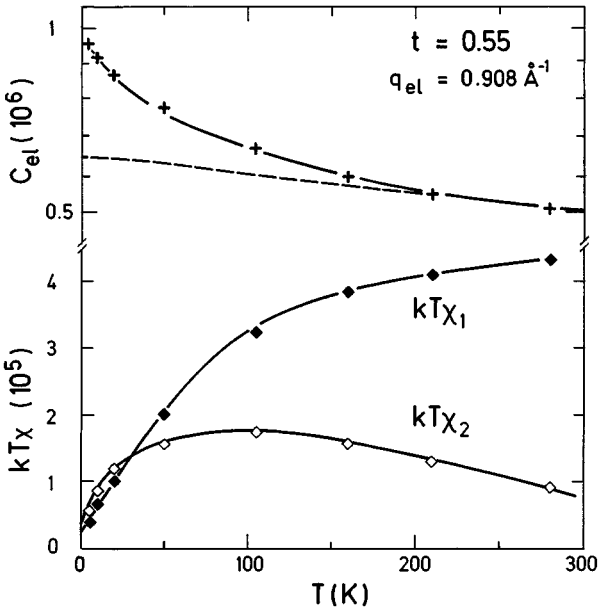

FIG. 10. Temperature dependence of the elastic intensity c_{el} and of the quasielastic intensities $kT\chi_1$ and $kT\chi_2$ for a q_{el} value of 0.908 $Å^{-1}$. The dashed line is the temperature variation of c_{el} expected from Debye-Waller effects (as deduced from neutron-diffraction data at the Bragg peak position).

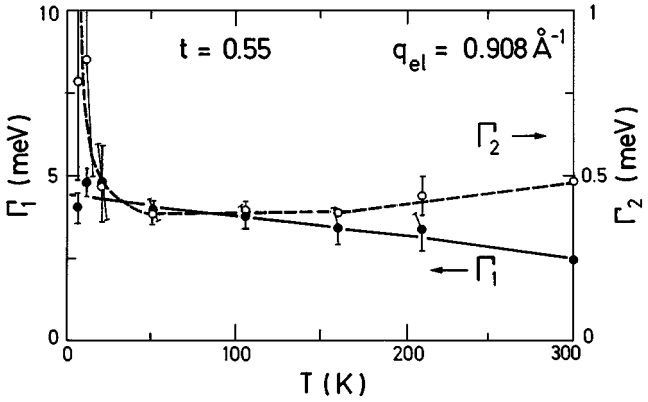

FIG. 11. Temperature dependence of the quasielastic widths Γ_1 and Γ_2 for a q_{el} value of 0.908 $Å^{-}$.

as the temperature decreases. This process gradually takes place from high temperatures, without showing anomalies at T_N or T_F. Surprisingly, the quasielastic widths do not decrease with temperature. This would have been expected in a conventional freezing process, if Γ_1 and Γ_2 were proportional to the inverse of the characteristic relaxation times. They are almost temperature independent down to T_F then seem to *increase* below T_F.

V. DISCUSSION

The above results suggest an inhomogeneous type of magnetism, with a wide range of correlation lengths, relaxation times, and energies for the spin excitations. We now propose a phenomenological description of the system, which displays three main temperature regimes. We first of all discuss the low- and zero-field behavior, then the influence of the applied field.

A. $T > T_N$

The inhomogeneous features of the paramagnetic phase are reminiscent of the so-called Griffith phase in diluted ferromagnets.[17] Neutron diffraction probes the existence of large, quasiordered regions, with a correlation length ξ which increases with decreasing temperature. It shows that some spins remain correlated up to about 3 T_N. Our unpublished polarized neutron measurements show that the sample strongly depolarizes the transmitted beam even above T_N, in contrast with usual paramagnets. Moreover, our field-cooled magnetization data, to be published later, suggest that a few spins remain frozen at very large time scales. The investigation of the paramagnetic phase at the different time scales probed by magnetic and neutron measurements, reveals a very large distribution of relaxation times and length scales for the spins correlations.

In the very short-time scale (10^{-11} s) of the inelastic neutron scattering, we cannot evidence any relaxation process in the temperature dependence of the quasielastic widths. This would have been shown by a decrease of $\Gamma(T)$. However, the elastic intensity strongly increases with decreasing T, and departs from the Debye-Waller curve even above T_N, which suggests slow relaxations, with a time scale greater than the experimental resolution. The behavior of the quasielastic

widths, which are almost T independent, is attributed to excitations of spins trapped in potential wells. The Γ values correspond to the typical energies of these excitations, namely to coupling constants similar to the rigidity of spin waves. The thermal population of the excitations decreases with decreasing T, which also contributes to the increase of the elastic intensity, at the expense of the quasielastic one. The excitation energies are not affected by the onset of the long-range correlations at T_N. As shown in the spin-glass sample ($t=0.7$), they are identical on the other side of the percolation threshold. Interestingly the highest energy Γ_1 corresponds to almost uncorrelated spins. A smaller energy Γ_2 is found corresponding to correlations on a larger scale ξ. The energy of the spin waves observed below T_N is even smaller, as discussed below.

B. $T_F<T<T_N$

At T_N, our unpublished low-field magnetization data show a strong increase of the susceptibility, (also evidenced by neutron depolarization), which does not obey usual ferrimagnetic scaling. Neutron data reveal the onset of rather long-range correlations, which contribute to the intensities of the Bragg peaks. Due to the limited q resolution, they only yield a lower limit for the ''Bragg'' length scale of about 150 Å. The absence of a critical behavior in zero field suggests that the ''Bragg'' correlations do not percolate through the sample. The static ordered domains created below T_N coexist and compete with the short-range spin correlations, whose dynamical nature is confirmed by the persistence of a paramagnetic component in the Mössbauer spectra. The growing of the Bragg intensity inhibits the short-range order. The diffuse intensity decreases and the associated correlation length saturates.

Spin waves may propagate within the medium,[11] but they are extremely damped, and their energy ($\omega<0.15$ meV for the sample $t=0.55$), remains much smaller than the energies of the local fluctuations Γ_1 and Γ_2. Below 100 K, the increasing frustration induces anomalies in the spin-wave spectrum: the stiffness constant decreases and the damping increases.

C. $T<T_F$

Below T_F ($T_F=25$ K), the Bragg intensity decreases, whereas the diffuse intensity and the finite correlation length increase. In the same temperature range, propagative excitations are no longer observed near the zone center: the spin waves strongly soften and become overdamped so that the corresponding signal becomes quasielastic. The excitations energies of the local fluctuations seem to increase.

All these features suggest a destabilization of the high-temperature state, and a new stabilization within a less ordered medium. As proposed by Aeppli *et al.*,[18] this could correspond to a breakdown of the static ordered domains into much smaller ones (of size ξ). However, several experimental facts favor the onset of a strongly locally canted state, without a significant decrease of the longitudinal correlation length. First of all, we do not observe any broadening of the Bragg peaks below T_F. Secondly, the M_0 value deduced from neutron data scales with the magnetization value even below T_F. Moreover, Mössbauer spectroscopy shows a strongly noncollinear behavior, even in magnetic fields higher than those required for the technical saturation of the sample.[4] The anomalies below T_F could therefore correspond to a crossover towards a more and more canted state, the correlation length of the diffuse scattering being associated with transverse-spin components.

D. Influence of the applied field

Above T_N, the applied field does not affect the dynamical correlations. Our recent magnetic measurements show that ferrimagnetic scaling is restored at T_N above 2 kOe, a field value comparable to that of the dipolar anisotropy field ($4\pi\rho M_0=1$ kOe). Below T_N, the spin components which contribute to the Bragg peaks are easily aligned by a field $H_{\rm sat}$, which corresponds to the technical saturation of the magnetic measurements. The temperature dependence of the Bragg intensity, and even its anomalous decrease below T_F, agrees with the ''spontaneous'' magnetization extrapolated from high fields. This shows that a field of the order of $H_{\rm sat}$ mostly aligns the static domains, in order to build a percolating network, but has little effect on the intrinsic frustration. The spins involved in the dynamical short-range correlations are very slowly aligned by the field. The correlation length measured between T_N and T_F decreases as $1/\sqrt{H}$, and the magnetization tends to saturate following the same law. Such a variation is predicted for the transverse correlation length of a ferromagnetic system perturbated by random fields,[19] or anisotropy fields.[20]

VI. CONCLUSION

The neutron experiments probe excitations with three different energy levels, corresponding to different spatial organizations. The strongest coupling corresponds to spins correlated on a very short length scale. The increase of the energies of the local fluctuations below T_F is reminiscent of observations in spin glasses.[21] The energy of the spin waves, which is much lower, show a maximum with temperature as in frustrated ferromagnets.[22] The result is the coexistence of both effects in the same sample.

Concomitantly with these dynamics, we observe a very peculiar behavior of the spin correlations. The main consequence of the frustration, i.e., the decrease of the Bragg intensity is also seen in other frustrated insulating systems like $Fe_{1-x}Mn_xTiO_3$,[23] $CdCr_{2(1-x)}In_{2x}S_4$ spinels,[24] or $YBa_2(Cu_{1-x}Fe_x)_3O_y$ ceramics.[25] It contrasts with the behavior of metallic systems, where a regime of weak frustration may be observed. In this latter regime, transverse-spin freezing may occur without any decrease of the longitudinal ordered component.[26]

The infinite range mean-field model[27] predicts three distinct transitions with decreasing temperature, and the persistence of longitudinal long-range order down to the lowest temperature. This model seems rather suitable to the weakly frustrated metals. Here, it clearly does not apply. The strong inhomogeneous character of the spinel sample, where different typical length and time scales coexist at the same temperature, could be expected for an insulating system close to the percolation threshold of the dominant interaction. We hope that our results will stimulate the improvement of existing theories, taking the actual structure of the system into account. We would like to make one suggestion. As concern-

ing the influence of frustration, mostly effective below T_N, local mean-field theories could be a good starting point. As stressed by Villain[1] in frustrated systems with short-range interactions, the conventional long-range order could be locally destroyed in strongly frustrated regions with the occurrence of canted local spins (CLS). These CLS induce a tilt of their surrounding neighbors by forming polarization clouds, so that a decrease of the mean magnetization may be expected at low temperature. The relevance of the local mean-field approach has been confirmed by Monte-Carlo simulations.[28] In the Villain model, the overlap of the polarization clouds leads to an effective long-range (dipole-dipole-like) interaction between the CLS. If the medium surrounding the clouds remains unperturbed, a true canting transition may be expected at a finite temperature. In our case, where the effective medium is strongly diluted and perturbed, one may expect a much stronger localization of the polarization clouds and a crossover transition towards a disordered canted state.

ACKNOWLEDGMENTS

We are strongly indebted to R. Kahn and F. Bourée for their help in the inelastic and neutron-diffraction measurements.

*Electronic address: mirebea@bali.saclay.cea.fr

[1] J. Villain, Z. Phys. B **33**, 31 (1979).
[2] Y. J. Uemura, A. Keren, K. Kojima, L. P. Le, G. M. Luke, W. D. Wu, Y. Ajiro, T. Asano, Y. Kuriyama, M. Mekata, H. Kikuchi, and K. Kakurai, Phys. Rev. Lett. **7**, 3306 (1994).
[3] L. Pytlick (unpublished).
[4] R. A. Brand, H. Georges-Gibert, J. Hubsch, and J. A. Heller, J. Phys. F **15**, 1987 (1985).
[5] G. Gavoille and J. Hubsch, J. Phys. (Paris) Colloq. **49**, C8-1159 (1988).
[6] F. Scholl and K. Binder, Z. Phys. B **39**, 239 (1980).
[7] J. Hubsch, G. Gavoille, and J. Bolfa, J. Appl. Phys. **49**, 1363 (1978).
[8] I. Mirebeau and M. Hennion, J. Magn. Magn. Mater. **140–144**, 1999 (1995).
[9] L. M. Corliss, J. M. Hastings, and F. G. Brockman, Phys. Rev. **90**, 1013 (1953).
[10] C. Haas, J. Phys. Chem. Solids **26**, 1225 (1965).
[11] J. M. Hastings and L. M. Corliss, Phys. Rev. B **126**, 556 (1962).
[12] G. Gavoille and J. Hubsch, J. Magn. Magn. Mater. **36**, 89 (1983).
[13] J. Hubsch and G. Gavoille, J. Magn. Magn. Mater. **66**, 17 (1987); **86**, 363 (1990).
[14] R. E. Watson and A. J. Freeman, Acta. Crystallogr. **14**, 27 (1961).
[15] C. G. Shull and M. K. Wilkinson, Phys. Rev. **97**, 304 (1955); W. Marshall, J. Phys C **2**, 88 (1968).
[16] P. G. de Gennes, J. Phys. Chem. Solids **4**, 223 (1958); P. G. de Gennes and J. Villain, *ibid*. **13**, 10 (1960); W. Marshall and S. W. Lovesey, *Theory of Thermal Neutron Scattering* (Oxford, Clarendon, 1971).
[17] A. J. Bray, Phys. Rev. Lett. **60**, 720 (1988).
[18] G. Aeppli, S. M. Shapiro, R. J. Birgenau, and H. S. Chen, Phys. Rev. B **28**, 5160 (1983).
[19] W. M. Saslow, Phys. Rev. B **35**, 3454 (1987).
[20] G. T. Rado, Phys. Rev. B **26**, 295 (1982); M. Steiner, KI. Kakurai, and J. K. Kjiems, Z. Phys. B **53**, 117 (1983).
[21] A. Murani, J. Phys. (Paris) **39**, 1517 (1978); C. Bellouard, M. Hennion, I. Mirebeau, and B. Hennion, J. Magn. Magn. Mater. **102**, 1627 (1992).
[22] B. Hennion, M. Hennion, F. Hippert, and A. P. Murani, J. Phys. F. **14**, 489 (1984); B. Hennion, M. Hennion, I. Mirebeau, and M. Alba, Phys. Rev. B **51**, 8204 (1995).
[23] H. Yoshisawa, S. Mitsuda, A. Aruga, and S. Ito, Phys. Rev. Lett. **59**, 2364 (1984); J. Phys. Soc. Jpn. **58**, 1416 (1989).
[24] S. Pouget, M. Alba, and M. Nogues, J. Magn. Magn. Mater. **140–144**, 1531 (1995); S. Pouget and M. Alba, J. Phys. C **7**, 4739 (1995).
[25] I. Mirebeau, C. Bellouard, M. Hennion, G. Jehanno, V. Caignaert, A. J. Dianoux, T. E. Phillips, and K. Moorjani, Physica C **184**, 299 (1991).
[26] I. Mirebeau, S. Itoh, S. Mitsuda, T. Watanabe, Y. Endoh, M. Hennion, and R. Papoular, Phys. Rev. B **41**, 11 405 (1990); I. Mirebeau, M. Hennion, S. Mitsuda, and Y. Endoh, in *Recent Progress in Random Magnets*, edited by D. H. Ryan (World Scientific, Singapore, 1992).
[27] M. Gabay and G. Toulouse, Phys. Rev. Lett. **47**, 201 (1981).
[28] W. M. Saslow and G. Parker, Phys. Rev. Lett. **56**, 1074 (1986); D. H. Ryan, in *Recent Progress in Random Magnets* (Ref. 26), p. 1.